Continuous production of magnetic iron oxide nanocrystals by oxidative precipitation

T. Asimakidou[a], A. Makridis[a], S. Veintemillas-Verdaguer[b], M.P. Morales[b], I. Kellartzis[c], M. Mitrakas[c], G. Vourlias[a], M. Angelakeris[a], K. Simeonidis[d,e,*]

[a] Department of Physics, Aristotle University of Thessaloniki, 54124 Thessaloniki, Greece
[b] Instituto de Ciencia de Materiales de Madrid, CSIC, Sor Juana Inés de la Cruz 3, Cantoblanco, 28049 Madrid, Spain
[c] Department of Chemical Engineering, Aristotle University of Thessaloniki, 54124 Thessaloniki, Greece
[d] Hephaestus Advanced Laboratory, Eastern Macedonia and Thrace Institute of Technology, 65404 Kavala, Greece
[e] Ecoresources P.C., Giannitson-Santaroza Str. 15-17, 54627 Thessaloniki, Greece

HIGHLIGHTS

- Industrial-scale preparation of low-cost magnetite nanoparticles.
- Transfer of laboratory synthesis to a continuous-flow process.
- Method based on oxidative precipitation of Fe^{2+} controlled by OH^- excess.
- Nanoparticles' dimensions range from 40 to 300 nm.
- Improved magnetic hyperthermia efficiency validated for developed nanoparticles.

GRAPHICAL ABSTRACT
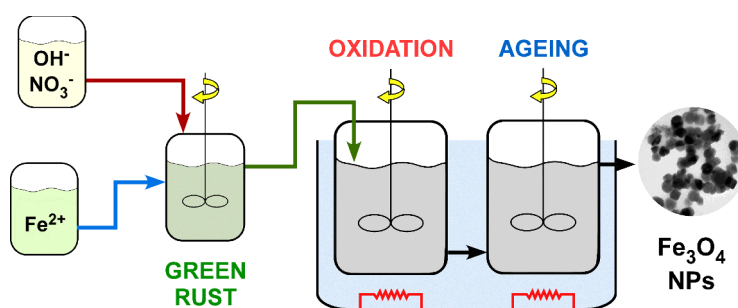
ABSTRACT

Continuous processes are always preferred over batch ones when reproducible and scalable industrial procedures are needed. This work illustrates the production of magnetite nanoparticles by oxidative precipitation in aqueous media, following a continuous approach that offers additional advantages. Particularly, the developed reaction setup succeeds (i) the complete separation of the green rust's precipitation from Fe_3O_4 nucleation, (ii) the achievement of constant concentrations in all ionic and solid forms throughout the production line when steady-state is reached, what means constant supersaturation from both the formation of green rust and Fe_3O_4, and (iii) the possibility to control critical parameters, such as OH^- excess over the initial stoichiometric $Fe(OH)_2$ precipitation, through on-line regulation of synthesis parameters such as the reactor's pH and redox potential. Importantly, continuous flow synthesis of Fe_3O_4 nanoparticles enables high production capacities, low energy consumption and proportional scale-up at any volume. As a proof of concept, obtained nanoparticles were evaluated according to their magnetic response as potential magnetic hyperthermia agents indicating significant improvement of heating efficiency that goes up to 1.5–2 kW/g_{Fe3O4} for both smaller (~40 nm) and larger (~200 nm) particles.

* Corresponding author at: Hephaestus Advanced Laboratory, Eastern Macedonia and Thrace Institute of Technology, 65404 Kavala, Greece.
  E-mail address: ksime@physics.auth.gr (K. Simeonidis).

1. Introduction

Engineered nanoparticles consisting of inorganic phases (metals, alloys, oxides, composites) stand out as an important class of nano-materials presenting wide chemical diversity and interesting electronic, optical, magnetic and mechanical properties while further opportunities arise by their size-induced coupling effects. Their role in our everyday-life gradually expands as more technological sectors, including manufactures, electronics, energy generation and storage, sensors, biomedicine, and environment processes, incorporate nanoparticles in order to improve efficiency [1–3]. Compatibility of the production of such materials with aqueous chemistry, which is the base of most industrial, environmental and biological processes, as well as the development of large-scale production schemes with low cost and good reproducibility, are key issues need to be addressed. Among inorganic nanoparticles, magnetic ones represent one of the most important materials characterized by their ability to respond to the application of an external magnetic field. This response enables their localization by Magnetic Resonance Imaging (MRI) and their use in therapy as drug carriers, biomolecule separation using a field gradient or as heat or mechanical damage sources using an alternating magnetic field [4]. In addition, several applications take advantage of their biocompatibility and chemical affinity (direct or induced by appropriate coatings) towards many molecules and ions resulting, for instance, in antimicrobial properties [5].

Magnetic iron oxide nanoparticles usually refer to those consisting of magnetite (Fe_3O_4) or maghemite (γ-Fe_2O_3) that combine facile and cheap preparation, chemical stability, biocompatibility, sufficient magnetism and wide range of sizes and morphologies available. The synthesis routes for such systems are based on the control of specific parameters (pH, temperature, pressure or redox potential), needed to generate a high supersaturated solution where nanoparticles nucleate. In addition, to achieve well-defined chemical composition, structural and colloidal stability, the nanoparticle synthesis usually involves protective coating by organic or inorganic molecules. However, the production of high quality nanoparticles rarely complies with green chemistry rules using organic solvents and expensive and toxic reagents combined with high reaction temperatures for long times. Such methods enable the production of small quantities of highly uniform nanoparticles with specific particle size and shape [6,7]. Besides, green synthetic methods using non-toxic reagents and low energy consumption, stand on the aqueous precipitation of iron salts with very low cost and high productivity, but they are restricted to a certain size range (below 15 nm) with wide size distribution. As a result, magnetite nanoparticles present modest magnetic response, and often favor the particle agglomeration with the consequent decrease in effective surface area and heating performance.

An interesting alternative for the production of iron oxide nanoparticles following a green route is the oxidative hydrolysis of Fe^{2+} in aqueous media. Thus, through the intermediate formation of green rust, uniform magnetite nanoparticles are obtained by completely separating the hydrolysis of iron (II) from dehydroxylation and oxidation of green rust [8]. Green rust refers to a class of mixed ferrous and ferric iron hydroxides based on the brucite $Fe(OH)_2$ layers where part of Fe^{2+} is oxidized to Fe^{3+} and anions and water molecules are in the inter-laminar space following the general formula $[Fe^{2+}_{(6-x)}Fe^{3+}_x(OH)_{12}]^{x+} \cdot [A_{x/n} \cdot yH_2O]^{x-}$, being A an n-valent anion such as Cl^-, CO_3^{2-} or SO_4^{2-} and y the number of interlayered water molecules crystallized in a layered double hydroxide structure. Mimicking natural processes during which green rust is a critical compound considered as a life-generation engine [9], the accurate control of reaction parameters is known to result in high purity and advanced crystallinity products with improved magnetic properties [10,11]. The role of oxidant's nature, the Fe^{2+} salt, the solvent, the pH and the temperature has been previously monitored in batch processes concluding $FeSO_4$, NaOH, $NaNO_3$ and ethanol/water as the combination of low-cost reagents that brings the

most stable green rust precursor following a lower dissociation rate when supersaturation is achieved [12]. However, carrying out the two-step process in a batch reactor involves a number of challenges arising from the time evolution of critical parameters such as the actual reagents and products concentration, the temperature and the pH during both processes. This is important not only for the reproducibility of the process but also for the energy consumption and the dimensions of the pilot plant needed for the synthesis. For instance, a large-scale production line would require a high-volume batch reactor and facilities to load the reaction mixture, significant power to heat the solution from room temperature up to nearly boiling temperature and non-negligible loss of time to evacuate, clean and reload the system. The long time needed for mixing and heating the reaction mixture in this pilot plant implicates the variation of critical parameters previously mentioned, and all will end up in an enhanced polydispersity of the product. On the contrary, continuous flow microfluidic reactors manage to overcome some of these difficulties and optimize nanoparticles characteristics compared to batch synthesis. Moreover, it is possible to receive unusual morphologies or phase combinations that cannot be achieved otherwise or introduce lab-on-a-chip devices to enable on-site synthesis [13–16]. Such processes take advantage of working in the steady state of a continuous flow mode, but their potential scale-up by assembling an extremely high number of microreactors working in parallel will imply additional difficulties and costs.

In spite of the fact that the demand of magnetic nanoparticles for developing applications is exponentially growing, not much effort has been devoted to investigate possibilities of transferring laboratory knowledge into large-scale production schemes. In an attempt to improve the conditions of synthesizing Fe_3O_4 nanoparticles and promote a process for their industrial-scale production, this work presents the continuous-flow version of the oxidative precipitation process able to operate under time-independent state in stationary condition. In order to fulfill this objective, we adapted the optimum critical parameters of the process determined previously using the batch approach to a continuous flow process. The design of the described process was implemented keeping in mind commonly adopted processes for the industrial production of iron oxides i.e. precipitation from salts into continuous stirred tank reactors (CSTR). More specifically, the oxidative precipitation of Fe^{2+} was performed in a sequence of two stirring reactors, in which the formation of the hydroxide gel and its ageing under mild oxidizing conditions are carried out separately. The role of the acidity during green rust production and the ethanol's presence were investigated, as well as the key parameters to define the geometrical characteristics and the magnetic properties of obtained nanoparticles. In order to test the validity of Fe_3O_4 nanoparticles as potential agents for biomedical practices, their efficiency in magnetically-triggered hyperthermia was examined.

2. Experimental

2.1. Product synthesis

Magnetite nanoparticles were prepared in a continuous-flow setup (Fig. 1) adapted to the reagents' proportions used for the synthesis of 22 nm Fe_3O_4 spherical nanoparticles in a batch [12], after dividing all concentrations by a factor of 10. Two separate 5 L tanks were used to store the reagent mixtures: one for the $FeSO_4 \cdot 7H_2O$ solution (0.03 M) and a second one for the mixture of $NaNO_3$ (0.06 M), NaOH (0.125 M) and ethanol (30% v/v when used). The tanks were periodically refilled by freshly dissolved reagents to feed the reactor. The solutions were pumped at a constant rate, 0.3 L/h and 1.2 L/h respectively, in a 0.5 L reactor operating at room temperature under mild mechanical stirring and intense nitrogen bubbling (residence period 20 min). Successful application of inert conditions in this part proved to be critical to completely inhibit oxidation by air and avoid formation of red-colored Fe^{3+} oxyhydroxides. The pH in this reactor was kept to a specific value
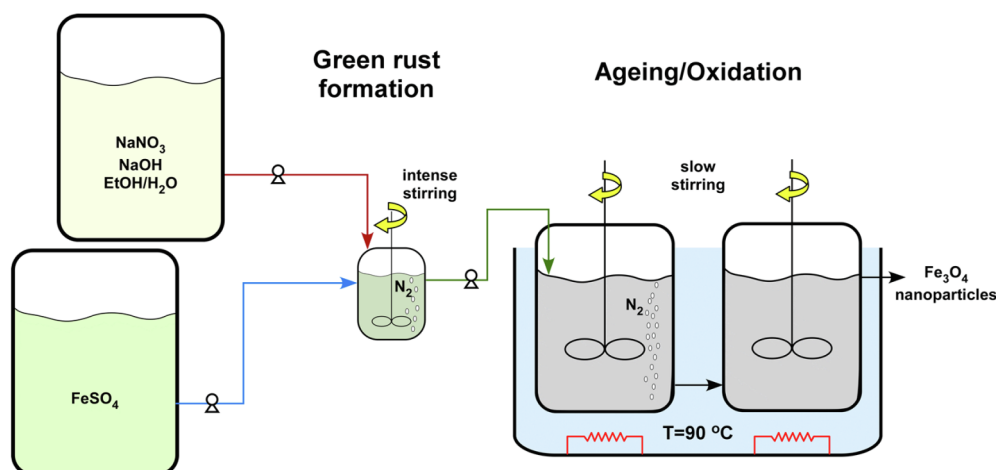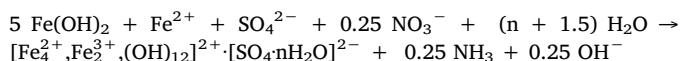
Fig. 1. Schematic representation of the laboratory continuous-flow process for the synthesis of Fe_3O_4 nanoparticles.
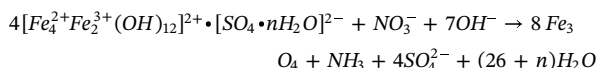
Table 1
Experimental parameters used for the Fe_3O_4 nanoparticles synthesis in the continuous-flow setup at 90 °C.

Sample	pH value		Solvent	[OH^-] decrease %
	Green rust	Final		
S1	12.5	12.0	H_2O/EtOH	63
S2	11.6	10.9	H_2O/EtOH	75
S3	10.8	10.1	H_2O/EtOH	79
S4	8.4	6.7	H_2O/EtOH	100
S5	12.3	12.1	H_2O	38
S6	11.3	11.0	H_2O	50
S7	10.1	9.8	H_2O	50
S8	9.2	6.7	H_2O	100

for each experiment by the periodical addition of drops of NaOH or H_2SO_4 solutions (one value in the range 8–12 ± 0.2 as shown in Table 1). In this reactor, the rapid formation of green rust takes place according to the reaction:

$$5\ Fe(OH)_2 + Fe^{2+} + SO_4^{2-} + 0.25\ NO_3^- + (n + 1.5)\ H_2O \rightarrow [Fe_4^{2+}, Fe_2^{3+}, (OH)_{12}]^{2+} \cdot [SO_4 \cdot nH_2O]^{2-} + 0.25\ NH_3 + 0.25\ OH^-$$

The green rust slurry was then pumped into the ageing reactor, consisting of two consecutive stirring tanks of 3 L each, placed into a water bath heated at 90 °C and surrounded by an insulating top to avoid water evaporation. In this way, green rust immediately meets maximum temperature avoiding the usual half-an-hour heating period in batch process. Relatively intense stirring and nitrogen bubbling is applied to the first reactor to homogenize the mixture whereas slow stirring is applied to the second one to allow better crystallization of the product. The total residence period in the ageing reactor was set at 4 h, equally split in each tank, and this value was used as the design parameter for the whole system. During ageing time, the reduction of nitrate ions caused the conversion of green rust to magnetite [17–19]:

$$4[Fe_4^{2+}Fe_2^{3+}(OH)_{12}]^{2+} \bullet [SO_4 \bullet nH_2O]^{2-} + NO_3^- + 7OH^- \rightarrow 8\ Fe_3$$
$$O_4 + NH_3 + 4SO_4^{2-} + (26 + n)H_2O$$

Finally, the black colored dispersion is collected in the outflow of the ageing reactor, cooled down to room temperature and then, washed several times with distilled water until a conductivity below 1 mS/cm was obtained. The pH during the production of the intermediate iron hydroxyl-sulfate and the presence of ethanol were used as the controlling parameter defining the reaction efficiency and the characteristics of obtained nanoparticles. In all cases, a drop of the pH was observed at the end of the ageing process as a consequence of the

oxidation pathway [12]. An overview of the synthesis parameters for the studied samples is presented in Table 1.

The relative decrease of the OH^- concentration (Table 1) is considered representative of the green rust's oxidation extend and increases in the presence of ethanol and at lower pH values. It should be explained that the OH^- decrease was estimated by the pH and the ionic product decrease and it is related to the weakening of hydrogen-bonding network and the reduction of dielectric constant in the case of ethanol, or the weakening of the green rust's stability in the case of the low starting pH.

2.2. Characterization

Structural-phase identification on dried samples was performed by powder X-ray diffractometry (XRD) using a water-cooled Rigaku Ultima + diffractometer with CuKa radiation, a step size of 0.05° and a step time of 3 s, operating at 40 kV and 30 mA. The diffraction patterns were compared to the Powder Diffraction Files (PDF) database [20] and the crystallite sizes were determined using the Scherrer's equation. The morphology and the mean particle size distributions were determined through transmission electron microscopy (TEM) images obtained using a JEOL JEM1010 microscope operating at 100 kV. Samples were prepared by placing a drop of the particles suspended in water onto a carbon coated copper grid and allowing it to dry at room temperature. The specific surface area of the nanoparticles was estimated by nitrogen gas adsorption at 77 K using a micropore surface area analyzer according to the Brunauer-Emmett-Teller (BET) model.

The ratio of Fe^{2+}/Fe^{3+} was determined by acid digestion of the nanoparticles and titration using $KMnO_4$ solution [21,22]. A sample quantity of 0.1 g was dissolved under heating in 50 mL 7 M H_2SO_4 (pretreated with nitrogen bubbling) and titrated with 0.05 M $KMnO_4$. The end point of the titration was defined by the persisting weak pink color, indicating that the MnO_4^- ions were no longer being reduced. Total iron content was measured after sample dissolution in HCl, by graphite furnace atomic absorption spectrophotometry using a Perkin Elmer AAnalyst 800 instrument.

2.3. Colloidal properties

A Zetasizer nano ZS by Malvern Instruments was used for the determination of the hydrodynamic size and the ζ-potential. The dynamic light scattering (DLS) allows the measurements of the aggregate size in dispersion among 0.6 and 6000 nm. A log-normal distribution function in intensity was used to fit the size data obtained. The Zetasizer nano ZS calculates the ζ-potential by determining the electrophoretic mobility using laser Doppler velocimetry and applying the Smoluchowski

approach. All the measurements were performed at room temperature using 0.001 M KNO_3 as background electrolyte and HNO_3 and KOH to change the suspension pH.

2.4. Magnetic measurements

A vibrating sample magnetometer MagLab VSM (Oxford Instrument) was used for the measurement of the magnetic properties up to a maximum field 1 T (~800 kA/m). Coercive field and saturation magnetization values were obtained from the hysteresis loops recorded at room temperature. The saturation magnetization values (M_s) expressed in Am^2/kg_{Fe3O4} were determined by extrapolating to infinite field the magnetization values in the linear region of M versus $1/H$. The corresponding minor loops measured after demagnetization at a maximum DC field 24 kA/m were also recorded as an indication of the AC field heating potential introduced by hysteresis losses.

2.5. Induction heating efficiency

Calorimetric measurements on the heating efficiency of nanoparticles under an AC magnetic field were acquired using a commercial converted 4.5 kW inductive heater at 765 kHz frequency and 24 kA/m magnetic field intensity. The specific loss power (SLP), or specific absorption rate (SAR) used to evaluate the heating performance was derived from the slope of the temperature versus time curve after subtracting water background signal and heat losses to the environment. Data are given in Watts per gram of Fe_3O_4. In addition, corresponding intrinsic loss power (ILP) was calculated after the expression $ILP = SLP/(f·H^2)$ with f and H being the AC frequency and the field intensity, respectively. Temperature was monitored by using an Opsens PicoM device with a GaAs-based fiber optic probe.

3. Results and discussion

All samples prepared in pure water and water/ethanol mixtures under different pH conditions (Table 1) by the continuous flow process present a ferrite iron oxide structure as shown in the XRD diagrams (Fig. 2). Chemical analysis identifies them as solid solutions of magnetite-maghemite but, considering the high Fe^{2+}/Fe^{3+} ratio, they will be called for short according to the dominant crystal phase which is magnetite (Table 2). It can be observed that below pH 10 (Samples 3, 4, 7, 8) the formation of iron oxy-hydroxides such as α-FeOOH was also

Fig. 2. XRD diagrams of samples prepared at pH 8.4–12.5 in H_2O/EtOH (S1-S4) and samples prepared at pH 9.2–12.3 in H_2O (S5-S8).

favored. This suggests that under these conditions the oxidation of green rust takes place more rapidly than its dehydroxylation and therefore, the complete transformation of intermediate products to magnetite does not occur. These intermediates and residual green rust are oxidized to α-FeOOH when the sample is exposed to the atmosphere [23]. Consequently, a reduction of the Fe^{2+}/Fe^{3+} ratio is observed in the samples prepared in pure water, as it is the case of sample 8 (Table 2). The average size of crystal domains for each sample was evaluated by applying the Scherrer's equation [24], on the broadening of (3 1 1) Fe_3O_4 peak (Table 2). These values were also compared to the actual particle size from microscopy observations to define the degree of polycrystallinity of the particles in each case. An improvement of the crystallinity is observed when the pH is around 10–11 reaching a maximum value of around 50 nm that falls off to less than half at synthesis pH around 7. Such finding shall be attributed to the modification of crystal growth mechanism as defined by the lower reaction rate of green rust at less alkaline environment.

On the other hand, the effect of reaction conditions during growth becomes more obvious in the geometry of the obtained nanoparticles. TEM images in Fig. 3 provide evidence about the different shape and dimensions of magnetite nanoparticles synthesized in continuous flow reactor. The most significant effect comes by the presence of ethanol which generally results in smaller nanocrystals in the range of 40–53 nm whereas pure water favors much larger particles in the range of 150–310 nm with higher polydispersity. Working at intense alkaline conditions in water/ethanol mixture enables the formation of almost spherical nanoparticles reaching a mean diameter of 53 nm at pH 12 and 43 nm at pH 11. At lower pH values, cubic-shaped nanocrystals dominate with a size of around 40 nm (diagonal dimension). On the contrary, nanoparticles grown in pure water achieve almost one order of magnitude larger dimensions forming well-defined nanocubes with their size strongly dependent on the synthesis pH. Particularly, at pH 12 the cube diagonal slightly overcomes 300 nm but gradually decreases below 200 nm at pH 10 [25,26]. It has been reported that magnetite nanocubes are favorable under small excess of OH^-, i.e. when all Fe^{2+} nucleates in the form of $Fe(OH)_2$. However, zero OH^- excess gives larger octahedral nanocrystals and Fe^{2+} excess produces larger spherical (even submicronic) particles [10]. Under neutral conditions (pH 7) close to the isoelectric point of magnetite, nanoparticles tend to agglomerate and a very polydisperse sample of spherical nanoparticles is obtained. It should be noted that rod-shaped formations observed in samples 4, 6 and 7 correspond to the α-FeOOH that appears as a synthesis byproduct, as confirmed by XRD [27].

In comparison to similar studies on the oxidative precipitation of magnetite nanocrystals in a batch reactor [12], particle sizes of the continuous-flow process appear to be significantly enlarged. For instance, magnetite formation using Na^+ and SO_4^{2-} as counterions in a 25% ethanol/water mixture was reported to result in monodisperse nanoparticles of 21.2 nm. The difference can be attributed to the nucleation process at iron concentrations ten times higher in the case of the batch reactor leading to a huge number of nuclei unable to grow further. The nucleation step is the initial precipitation of ferrous ions in green rust that serves as substrate for the magnetite nanoparticles growth by means of oxidation, dehydration and co-precipitation. The ten times reduction of concentration of iron with respect to previous batch experiments caused a smaller nucleation rate. The smaller number of nuclei formed leads in larger particles [28]. As a consequence, the corresponding dimensions of nanocrystals prepared by the continuous-flow system are almost double in size (40–50 nm). Compared to similar batch synthesis, the polydispersity index for continuous-flow system appears slightly smaller lying in the range of 0.10–0.15. It should be underlined that the described low-concentration effect only partially explains the observed size variation since batch synthesis at the same concentrations than the continuous-flow procedure, indicated a small drop of the size for S1, ~43 nm (Supporting information). This is an evidence about the significant role of setting
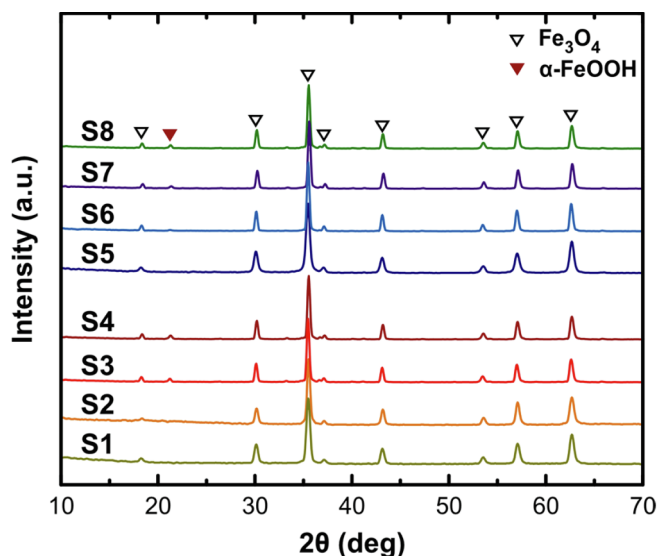
Table 2
Overview of the physical, chemical and morphological properties of the samples produced in the continuous-flow system.

Sample	Solvent	Shape	Size (nm)	Crystal size (nm)	BET (m²/g)	Fe²⁺/Fe³⁺	M_s (Am²/kg)
S1	H_2O/EtOH	Sphere	53 ± 7.7	29.2	30	0.45	79.5
S2	H_2O/EtOH	Sphere	43 ± 6.7	32.1	32	0.47	85.6
S3	H_2O/EtOH	Cubic	39 ± 6.1	42.7	34	0.44	82.7
S4	H_2O/EtOH	Cubic	40 ± 6.6	31.0	33	0.37	82.3
S5	H_2O	Cubic	310 ± 28.6	45.6	16	0.42	76.6
S6	H_2O	Cubic	260 ± 24.5	54.8	12	0.42	90.0
S7	H_2O	Cubic	190 ± 25.9	55.5	15	0.37	90.2
S8	H_2O	Sphere	150 ± 21.8/280 ± 28.9	24.1	14	0.28	56.3
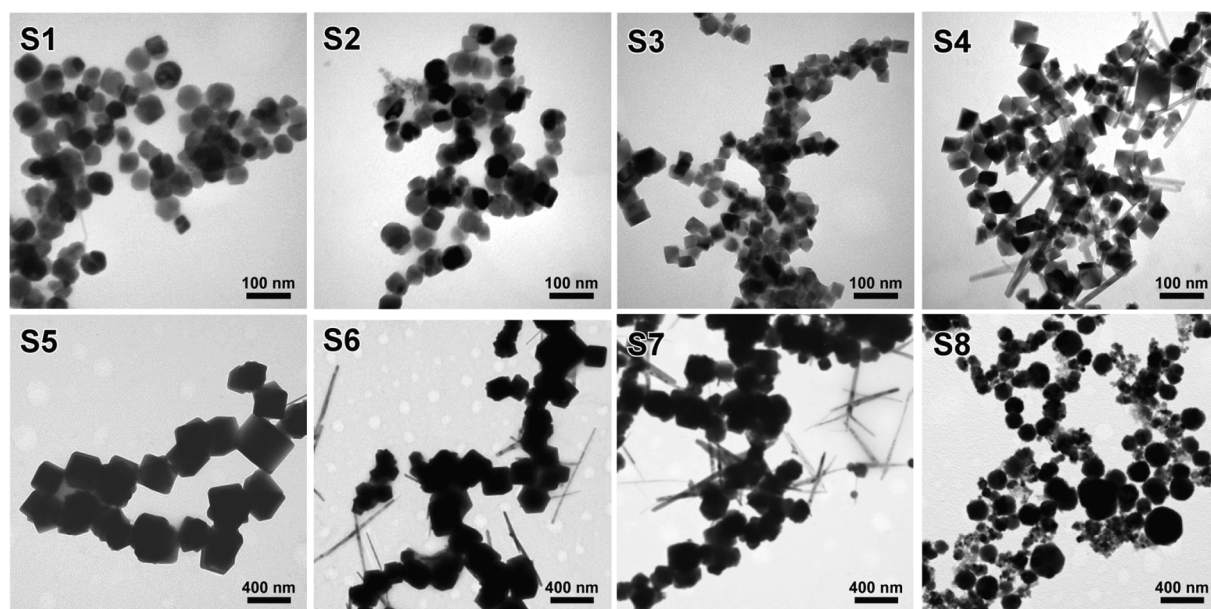
Fig. 3. TEM images of samples prepared at pH 8.4–12.5 in H_2O/EtOH (S1-S4) and samples prepared at pH 9.2–12.3 in H_2O (S5-S8) by the continuous-flow system. Note the differences in scale bars in the two rows.
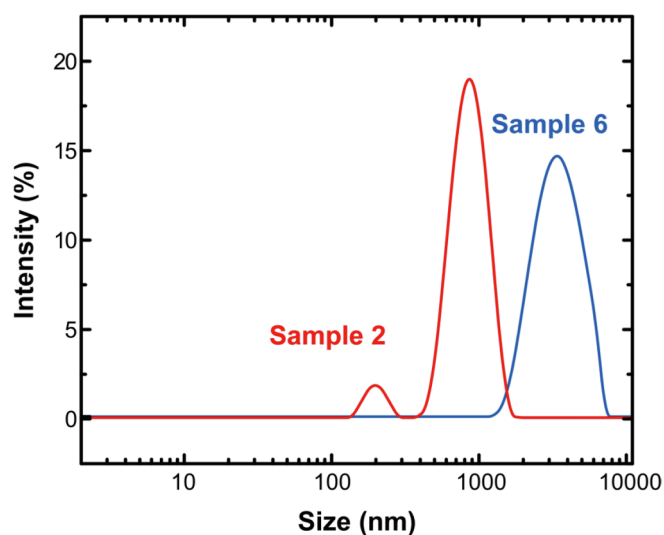

Fig. 4. Hydrodynamic size calculated by DLS measurements of the colloidal suspensions of magnetic nanoparticles prepared at pH 11 in the continuous-flow system.

the reaction parameters as time-independent in the continuous-flow setup, in the nucleation/growth mechanism.

The differences get even higher in pure water synthesis when the nanoparticles size goes from 36.9 nm in a batch reactor at ten times higher iron concentrations or 55 nm at similar concentrations, up to 190 nm in the continuous-flow system. Here, key parameters related to the growth step dominate, i.e. the transformation of green rust to magnetite. Thus, the use of water affects the speciation of precipitating ionic forms and, as a result, oxidation and dehydroxylation rate. When the pH increases, larger quantities of Na^+ and OH^- are included in the layered double hydroxide structure of the green rust leading to larger magnetite particles [29]. It should be mentioned that under less alkaline conditions, there is a tendency to produce intermediate products such as lepidocrocite (γ-FeOOH) or goethite (α-FeOOH), especially for samples synthesized in pure water [30]. On the other hand, oxidation-dehydroxylation of the initially formed green rust proceeds under very low Fe^{2+} and green rust concentrations, very high residual sulfate concentrations and in the presence of formed magnetite nanocrystals. Such parameters allow a slow reaction rate probably heterogeneously-assisted on the surface of existing nanoparticles and therefore, larger particles are attained compared to a similar batch reaction.

In accordance to the size of synthesized magnetite nanocrystals in the continuous-flow system, the specific surface area of the samples prepared in the water/ethanol mixture is in the range of 30–35 m²/g but decreases to around half of this value for the samples grown in pure water (12–16 m²/g). When samples are dispersed in water forming a colloidal suspension, the actual organization of the nanoparticles in aggregates is reflected in the DLS measurements concerning the hydrodynamic diameter (Fig. 4). Samples grown in pure water generally form larger aggregates with a mean hydrodynamic size of 2400 nm, in particular for the sample synthesized at pH 11. The corresponding sample produced in water-ethanol mixture show smaller hydrodynamic
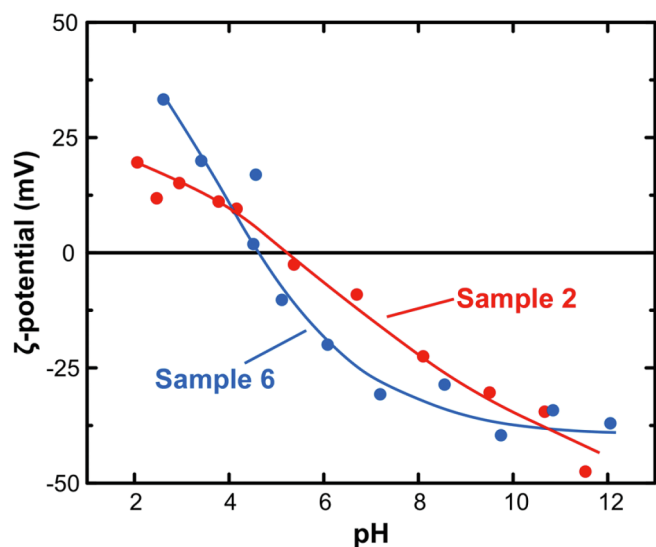
Fig. 5. Zeta-potential measurements of samples prepared at pH 11 in the continuous-flow system.

diameters with a bimodal distribution with peaks located at 170 and 780 nm.

The effective surface charge of the obtained nanoparticles in aqueous colloidal suspensions was signified by the electrophoretic mobility measurements at different pH values. Fig. 5 presents the ζ-potential curves for nanoparticles prepared at pH 11 in water-ethanol mixture (sample 2) and pure water (sample 6). Isoelectric points for both samples were found to be shifted below pH 5.5 indicating the important role of OH^- and SO_4^{2-} excess in the determination of a negatively-charged particle surface through their favorable adsorption. In the absence of ethanol, the surface modification effect is more intense and the nanoparticles show a lower isoelectric point (pH 4.7) compared to the smaller nanocrystals produced in water-ethanol (pH 5.3). Similar results concerning the contribution of ethanol in the stabilization of surface charge were observed for magnetite nanoparticles prepared by the oxidative precipitation of Fe(II) sulfate in a batch [10]. Interestingly, a typical nanoparticles dispersion (1 g/L) has a time window of colloidal stability of up to 1 h.

The magnetic properties of the obtained nanoparticles are consistent with the presence of a well-defined magnetite structure and the stoichiometric Fe^{2+}/Fe^{3+} ratio. All samples follow a ferrimagnetic behavior at room temperature which is reasonable for nanoparticles lying well-above the superparamagnetic limit for magnetite (> 20 nm). More specifically, the saturation magnetization estimated from the hysteresis loops (Supporting information) is equal to the reported values for bulk magnetite for many samples [31]. An important deviation to lower magnetization values is observed for nanoparticles grown in pure water and at low pH values (sample 8). As mentioned, the crystal growth mechanism is deteriorated when working at neutral pH values resulting in a polydispersed system containing iron oxy-hydroxides. Coercive field shows non-zero values varying within a narrow range 6.4–8 kA/m.

Fig. 6 shows a comparison of the minor loops obtained for samples synthesized in water/ethanol and pure water at a maximum field equal to the field applied in the magnetic hyperthermia experiments of this work (24 kA/m). Although measurements were taken in DC field, it has been shown that the integration of the area included in the loops is in general proportional to the expected heating efficiency when hysteresis losses are the main heating mechanism at the radiofrequency AC fields used in magnetic hyperthermia. In this case, samples prepared under strong alkaline conditions provide the larger hysteresis area. In particular, sample 5 (pH 12 in water) brings the maximum value approaching 170 J/g whereas samples 1 and 2 (pH 12 and 11 in water/ethanol) show similar large hysteresis areas, reaching 110 and 150 J/g,
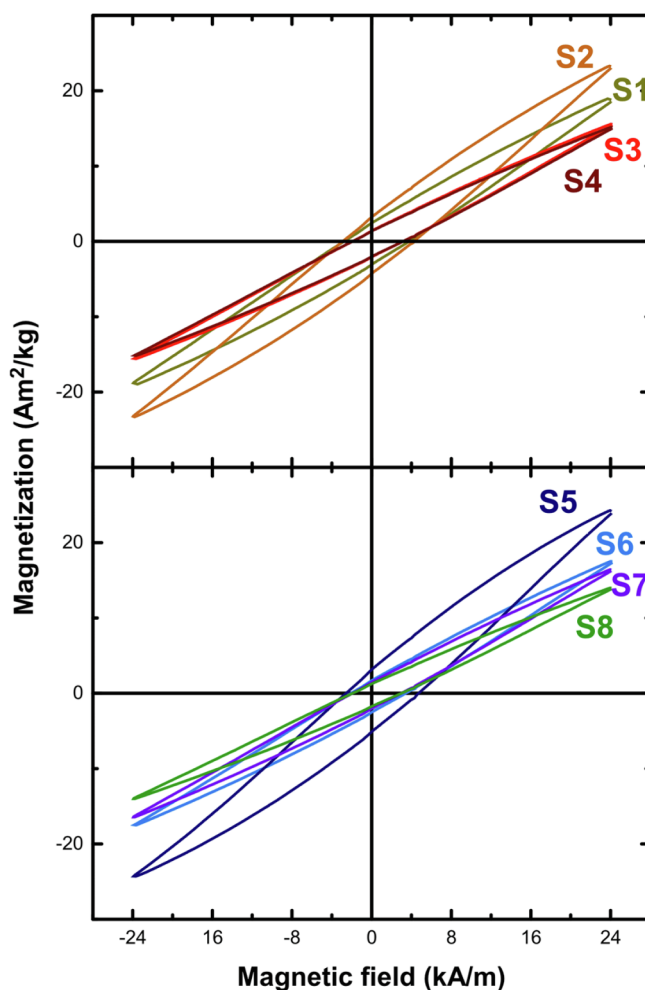

Fig. 6. Minor magnetic hysteresis loops at maximum field 24 kA/m for the studied samples prepared in the continuous-flow system.

respectively. For the rest of the samples, hysteresis areas within the range 50–80 J/g were measured.

The comparison of the hysteresis areas of the minor loops measured in powders and the SLP values estimated by temperature versus time curves in dispersions of the magnetite nanocrystals are shown in Fig. 7. It is very interesting to see that SLP values obtained under an AC magnetic field are directly proportional to the hysteresis areas obtained from a DC magnetic measurement suggesting hysteresis losses as the dominant mechanism of heat generation. Such finding is reasonable considering that the dimensions are well above the superparamagnetic limit, i.e. within the monodomain range 20–70 nm (water/ethanol) or in the multi-domain range, > 70 nm (pure water) and their behavior is clearly ferrimagnetic.

Importantly, the heating efficiency for the nanoparticles prepared under strong alkaline conditions is among the highest ones reported for single-phase magnetite particles developed by the oxidative precipitation method, with SLP values overcoming 1 kW/g or even higher, as it is the case of sample 5 whose SLP approaches 2 kW/g with respect to Fe_3O_4 mass. For comparison, the corresponding samples prepared in a batch resulted in SLP values lower than 0.5 kW/g (708 kHz, 24 mT) [12]. These differences are less significant when measuring the SLP at lower frequencies and field strengths, going down by one order of magnitude [10,32] (check Supporting Information). It should be noted that much higher heating efficiencies, even overcoming 10 kW/g, have been reported for combinations of Co, Zn, Mn prepared by organic synthesis [33–35]. However, those synthesis methods cannot be defined as green and low-cost, because of the presence of potentially toxic
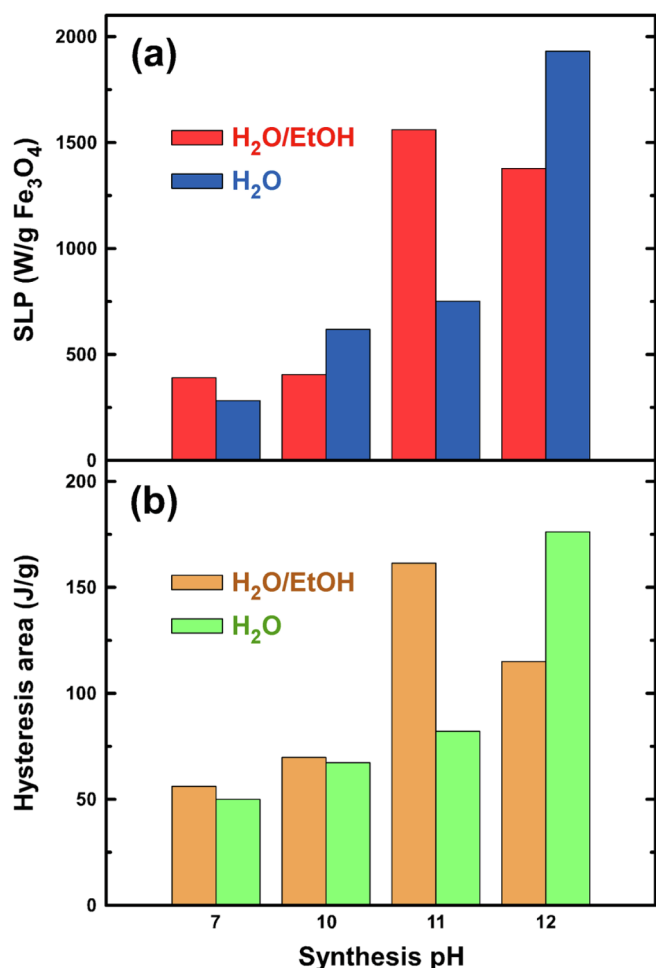
Fig. 7. Specific loss power dependence with synthesis pH and solvent for magnetite nanoparticle colloidal suspensions prepared by continuous-flow system, measured at 24 kA/m and 765 kHz (a). Corresponding magnetic hysteresis area estimated by minor loops up to 24 kA/m at room temperature (b).

nanoparticles since all reaction parameters are fixed at any stage and complete homogenization is achieved. Furthermore, the "extracted" parameters by the continuous flow synthesis of 0.7 g Fe_3O_4/h enable the design of a full-scale unit for the production of huge quantities by just multiplying the tanks' volumes and the flowrates. New industrial applications of magnetite nanoparticles in catalysis, biotechnology, water remediation, etc. or in general, in the area of environmental remediation, which is a subject of growing interest due to the superior performance of nanomaterials compared to conventional technologies, could benefit from this work.

Declaration of Competing Interest

The authors declare that they have no known competing financial interests or personal relationships that could have appeared to influence the work reported in this paper.

Acknowledgements

Appendix A. Supplementary data

Supplementary data to this article can be found online at https:// doi.org/10.1016/j.cej.2020.124593.

References

[1] M. Colombo, S. Carregal-Romero, M.F. Casula, L. Gutiérrez, M.P. Morales, I.B. Böhm, J.T. Heverhagen, D. Prosperi, W.J. Parak, Biological applications of magnetic nanoparticles, Chem. Soc. Rev. 41 (2012) 4306, https://doi.org/10.1039/ c2cs15337h.

[2] K. Simeonidis, C. Martinez-Boubeta, P. Zamora-Pérez, P. Rivera-Gil, E. Kaprara, E. Kokkinos, M. Mitrakas, Implementing nanoparticles for competitive drinking water purification, Environ. Chem. Lett. 17 (2019) 705–719, https://doi.org/10. 1007/s10311-018-00821-5.

[3] D.V. Talapin, J.S. Lee, M.V. Kovalenko, E.V. Shevchenko, Prospects of colloidal nanocrystals for electronic and optoelectronic applications, Chem. Rev. 110 (2010) 389–458, https://doi.org/10.1021/cr900137k.

[4] Nguyen T.K. Thanh (Ed.), Clinical Applications of Magnetic Nanoparticles: Design to Diagnosis Manufacturing to Medicine, first ed., CRC Press, Boca Raton, 2018.

[5] H. Maleki, A. Rai, S. Pinto, M. Evangelista, R.M.S. Cardoso, C. Paulo, T. Carvalheiro, A. Paiva, M. Imani, A. Simchi, L. Durães, A. Portugal, L. Ferreira, High antimicrobial activity and low human cell cytotoxicity of core-shell magnetic nanoparticles functionalized with an antimicrobial peptide, ACS Appl. Mater. Interfaces 8 (2016) 11366–11378, https://doi.org/10.1021/acsami.6b03355.

[6] G. Salas, C. Casado, F.J. Teran, R. Miranda, C.J. Serna, M.P. Morales, Controlled synthesis of uniform magnetite nanocrystals with high-quality properties for biomedical applications, J. Mater. Chem. 22 (2012) 21065, https://doi.org/10.1039/ c2jm34402e.

[7] B.H. Kim, N. Lee, H. Kim, K. An, Y. Il Park, Y. Choi, K. Shin, Y. Lee, S.G. Kwon, H. Bin Na, J.-G. Park, T.-Y. Ahn, Y.-W. Kim, W.K. Moon, S.H. Choi, T. Hyeon, Large-scale synthesis of uniform and extremely small-sized iron oxide nanoparticles for high-resolution T1 magnetic resonance imaging contrast agents, J. Am. Chem. Soc. 133 (2011) 12624–12631, https://doi.org/10.1021/ja203340u.

[8] T. Sugimoto, E. Matijević, Formation of uniform spherical magnetite particles by crystallization from ferrous hydroxide gels, J. Colloid Interface Sci. 74 (1980) 227, https://doi.org/10.1016/0021-9797(80)90187-3.

[9] M.J. Russell, Green rust: the simple organizing 'seed' of all life? Life 8 (2018), https://doi.org/10.3390/life8030035.

elements for biomedical applications [36]. Lower but not negligible values in the range 0.25–0.75 kW/g were measured for samples prepared at less alkaline environments. The ILP index for the most efficient samples was found between 3 and 4.4 nH·m^2/kg whereas samples prepared at less alkaline conditions presented values in the range 0.6–1.4 nH·m^2/kg.

Therefore, regarding magnetic hyperthermia as an application of major interest for magnetite nanoparticles, optimum conditions for its synthesis in water/ethanol mixture is the use of a pH above 11, while when working in pure water, the pH should be adjusted to 12. It must be underlined that the obtained nanoparticles in pure water are almost one order of magnitude larger than those for water/ethanol, limiting the potential applicability in biomedical uses. Other important applications of these nanoparticles are now under study such as catalysis or water remediation [37–39].

4. Conclusions

The continuous flow process developed in this work allows the preparation of uniform magnetite nanoparticles with sizes between 40 and 300 nm and very interesting magnetic properties. The continuous operation using the proposed concentrations and flowrates resulted in narrow dispersion of properties, using reagents that are non-toxic or substantially less toxic and an important reduction in waste generation in comparison to other synthesis methods in batches. Importantly, the system may operate uninterruptedly providing reproducible

[10] M.A. Verges, R. Costo, A.G. Roca, J.F. Marco, G.F. Goya, C.J. Serna, M.P. Morales, M. Andrés Vergés, R. Costo, A.G. Roca, J.F. Marco, G.F. Goya, C.J. Serna, M.P. Morales, Uniform and water stable magnetite nanoparticles with diameters around the monodomain-multidomain limit, J. Phys. D-Appl. Phys. 41 (2008) 134003.

[11] M.A. Gonzalez-Fernandez, T.E. Torres, M. Andrés-Vergés, R. Costo, P. de la Presa, C.J. Serna, M.P. Morales, C. Marquina, M.R. Ibarra, G.F. Goya, Magnetic nanoparticles for power absorption: optimizing size, shape and magnetic properties, J. Solid State Chem. 182 (2009) 2779–2784, https://doi.org/10.1016/j.jssc.2009.07.047.

[12] Y. Luengo, M.P. Morales, L. Gutiérrez, S. Veintemillas-Verdaguer, Counterion and solvent effects on the size of magnetite nanocrystals obtained by oxidative precipitation, J. Mater. Chem. C 4 (2016) 9482–9488, https://doi.org/10.1039/C6TC03567A.

[13] C.D. Ahrberg, J.W. Choi, B.G. Chung, Droplet-based synthesis of homogeneous magnetic iron oxide nanoparticles, Beilstein J. Nanotechnol. 9 (2018) 2413–2420, https://doi.org/10.3762/bjnano.9.226.

[14] G. Salazar-Alvarez, M. Muhammed, A.A. Zagorodni, Novel flow injection synthesis of iron oxide nanoparticles with narrow size distribution, Chem. Eng. Sci. 61 (2006) 4625–4633, https://doi.org/10.1016/j.ces.2006.02.032.

[15] W. Glasgow, B. Fellows, B. Qi, T. Darroudi, C. Kitchens, L. Ye, T.M. Crawford, O.T. Mefford, Continuous synthesis of iron oxide (Fe3O4) nanoparticles via thermal decomposition, Particuology 26 (2016) 47–53, https://doi.org/10.1016/j.partic.2015.09.011.

[16] L. Uson, M. Arruebo, V. Sebastian, J. Santamaria, Single phase microreactor for the continuous, high-temperature synthesis of < 4 nm superparamagnetic iron oxide nanoparticles, Chem. Eng. J. 340 (2018) 66–72, https://doi.org/10.1016/j.cej.2017.12.024.

[17] J.T. Moraghan, R.J. Buresh, Chemical reduction of nitrite and nitrous oxide by ferrous iron, Soil Sci. Soc. Am. J. 41 (1977) 47, https://doi.org/10.2136/sssaj1977.03615995004100010017x.

[18] H.C.B. Hansen, O.K. Borggaard, J. Sørensen, Evaluation of the free energy of formation of Fe(II)-Fe(III) hydroxide-sulphate (green rust) and its reduction of nitrite, Geochim. Cosmochim. Acta 58 (1994) 2599–2608, https://doi.org/10.1016/0016-7037(94)90131-7.

[19] H.C.B. Hansen, C.B. Koch, H. Nancke-Krogh, O.K. Borggaard, J. Sørensen, Abiotic nitrate reduction to ammonium: Key role of green rust, Environ. Sci. Technol. 30 (1996) 2053–2056, https://doi.org/10.1021/es950844w.

[20] Joint Center for Powder Diffraction Studies, ed., Powder Diffraction File, 2004t ed., International Centre for Diffraction Data, Newtown Square, PA, (n.d.).

[21] S.J. Kemp, R.M. Ferguson, A.P. Khandhar, K.M. Krishnan, Monodisperse magnetite nanoparticles with nearly ideal saturation magnetization, RSC Adv. 6 (2016) 77452–77464, https://doi.org/10.1039/c6ra12072e.

[22] G.M. da Costa, C. Blanco-Andujar, E. De Grave, Q.A. Pankhurst, Magnetic nanoparticles for in vivo use: a critical assessment of their composition, J. Phys. Chem. B 118 (2014) 11738–11746, https://doi.org/10.1021/jp5055765.

[23] Y. Tamaura, P.V. Buduan, T. Katsura, Studies on the oxidation of iron(II) ion during the formation of Fe3O4 and α-FeO(OH) by air oxidation of Fe[OH]2 suspensions, J. Chem. Soc., Dalt. Trans. 1807–1811 (1981), https://doi.org/10.1039/DT9810001807.

[24] A.L. Patterson, The Scherrer formula for X-ray particle size determination, Phys. Rev. 56 (1939) 978–982, https://doi.org/10.1103/PhysRev.56.978.

[25] A. Géhin, C. Ruby, M. Abdelmoula, O. Benali, J. Ghanbaja, P. Refait, J.M.R. Génin, Synthesis of Fe(II-III) hydroxysulphate green rust by coprecipitation, Solid State Sci. 4 (2002) 61–66, https://doi.org/10.1016/S1293-2558(01)01219-5.

[26] C. Ruby, A. Upadhyay, A. Géhin, G. Ona-Nguema, J.-M.R. GÉnin, In situ redox flexibility of FeII-III oxyhydroxycarbonate green rust and fougerite, Environ. Sci. Technol. 40 (2006) 4696–4702, https://doi.org/10.1021/es0606834.

[27] C. Pantke, M. Obst, K. Benzerara, G. Morin, G. Ona-Nguema, U. Dippon, A. Kappler, Green rust formation during Fe(II) oxidation by the nitrate-reducing *Acidovorax* sp. strain BoFeN1, Environ. Sci. Technol. 46 (2012) 1439–1446, https://doi.org/10.1021/es2016457.

[28] J.W. Mullin, Crystallization, fourth ed., Butterworth-Heinemann, Oxford, UK, 2001.

[29] A. Al Mamun, A. Onoguchi, G. Granata, C. Tokoro, Role of pH in green rust preparation and chromate removal from water, Appl. Clay Sci. 165 (2018) 205–213, https://doi.org/10.1016/j.clay.2018.08.022.

[30] M. Usman, J.M. Byrne, A. Chaudhary, S. Orsetti, K. Hanna, C. Ruby, A. Kappler, S.B. Haderlein, Magnetite and green rust: synthesis, properties, and environmental applications of mixed-valent iron minerals, Chem. Rev. 118 (2018) 3251–3304, https://doi.org/10.1021/acs.chemrev.7b00224.

[31] B.D. Cullity, C.D. Graham, Introduction to Magnetic Materials, John Wiley & Sons Inc, Hoboken, NJ, USA, 2008, , https://doi.org/10.1002/9780470386323.

[32] M. Marciello, V. Connord, S. Veintemillas-Verdaguer, M.A. Vergés, J. Carrey, M. Respaud, C.J. Serna, M.P. Morales, Large scale production of biocompatible magnetite nanocrystals with high saturation magnetization values through green aqueous synthesis, J. Mater. Chem. B 1 (2013) 5995, https://doi.org/10.1039/c3tb20949k.

[33] S.H. Moon, S.H. Noh, J.H. Lee, T.H. Shin, Y. Lim, J. Cheon, Ultrathin interface regime of core-shell magnetic nanoparticles for effective magnetism tailoring, Nano Lett. (2017), https://doi.org/10.1021/acs.nanolett.6b04016.

[34] S.H. Noh, W. Na, J.T. Jang, J.H. Lee, E.J. Lee, S.H. Moon, Y. Lim, J.S. Shin, J. Cheon, Nanoscale magnetism control via surface and exchange anisotropy for optimized ferrimagnetic hysteresis, Nano Lett. 12 (2012) 3716–3721, https://doi.org/10.1021/nl301499u.

[35] J.-H. Lee, J.-T. Jang, J.-S. Choi, S.H. Moon, S.-H. Noh, J.-W. Kim, J.-G. Kim, I.-S. Kim, K.I. Park, J. Cheon, Exchange-coupled magnetic nanoparticles for efficient heat induction, Nat. Nanotechnol. 6 (2011) 418–422, https://doi.org/10.1038/nnano.2011.95.

[36] S.H. Moon, S. Noh, J.-H. Lee, T.-H. Shin, Y. Lim, J. Cheon, Correction to ultrathin interface regime of core–shell magnetic nanoparticles for effective magnetism tailoring, Nano Lett. 17 (2017), https://doi.org/10.1021/acs.nanolett.7b01759.

[37] A. Pratt, Environmental applications of magnetic nanoparticles, Front. Nanosci. 6 (2014) 259–307, https://doi.org/10.1016/B978-0-08-098353-0.00007-5.

[38] S.C.N. Tang, I.M.C. Lo, Magnetic nanoparticles: essential factors for sustainable environmental applications, Water Res. 47 (2013) 2613–2632, https://doi.org/10.1016/j.watres.2013.02.039.

[39] A.-H. Lu, E.L. Salabas, F. Schüth, Magnetic nanoparticles: synthesis, protection, functionalization, and application, Angew. Chemie Int. Ed. 46 (2007) 1222–1244, https://doi.org/10.1002/anie.200602866.